Circular Cylinder Response to Kármán Vortex Shedding

L. E. Ericsson*
Lockheed Missiles & Space Company, Sunnyvale, California

A new method for computation of the response of structural members of circular cross section to Kármán vortex shedding is presented. In contrast to existing methods, which are based solely on mathematical concepts with little regard to the existing fluid dynamics, the present method is based on realistic unsteady flow concepts previously applied to the analysis of dynamic airfoil stall. The method is shown to give predictions that are in excellent agreement with experimental results.

Nomenclature

D = cylinder diameter
f = frequency of oscillating body
f_o = natural frequency of oscillating body
f_p = frequency of pressure oscillation
f_v = frequency of Kármán vortex shedding
f_{v0} = f_v for stationary flow conditions
l = sectional lift: coefficient $c_l = l/(p_\infty U_\infty^2/2)$
p = static pressure: coefficient $C_p = (p - p_\infty)/(\rho_\infty U_\infty^2/2)$
Re = Reynolds number, $= U_\infty D/\nu_\infty$
S = Strouhal number, $= fD/U_\infty$
t = time
U = horizontal velocity
$\bar{U}_c$ = convection velocity
$\bar{U}_1 U_\infty$ = unsteady velocity amplitude
$\bar{U}_0 U_\infty$ = time-average velocity
$\bar{V}$ = reduced velocity, $= S^{-1}$
z = translatory coordinate
δ^* = boundary-layer displacement thickness
Δ = increment and single amplitude
ϵ = small quantity
ζ_0 = mechanical damping, fraction or critical
θ = boundary-layer momentum thickness
κ_w = wall velocity ratio, $= (|U_w|/U_e)/(|\dot{z}|/U_\infty)$
ν = kinematic viscosity
ρ = fluid density
ϕ = phase angle
φ = peripheral angular cordinate, = 0 at the stagnation point
$\omega, \bar{\omega}$ = oscillation frequency; $\omega = 2\pi f$, $\bar{\omega} = \omega D/U_\infty = 2\pi S$

Subscripts

B = base
e = edge of boundary layer
lim = limit cycle amplitude
m = maximum amplitude
max = maximum
s = flow separation
w = wall
1,2 = numbering subscripts
∞ = undisturbed flow

Superscripts

$\bar{(\ )}$ = integrated mean value, e.g., $\bar{U}_e$ in Eq. (14)
$(\ )'$ = fluctuating quantity, e.g., p'

Derivative Symbols

$\dot{z}$ = $\partial z/\partial t$: $c_{l\dot{z}} = \partial c_l/\partial(\dot{z}/U_\infty)$

Presented as Paper 86-0999 at the AIAA/ASME/ASCE/AHS 27th Structures, Structural Dynamics and Materials Conference, San Antonio, TX, May 19-21, 1986; received July 7, 1986; revision received April 29, 1987.

*Senior Consulting Engineer. Fellow AIAA.

Introduction

BEAMS with circular cross sections commonly are used in structures exposed to winds and sea currents. Despite the obvious fact that the fluid mechanics must play a dominant role, most existing methods for computation of the lateral cylinder response to Kármán vortex shedding are based solely on mathematical concepts with little regard to the fluid dynamics.

In the present paper, the detailed measurements by Furguson[1] and Furguson and Parkinson[2] are used, together with unsteady flow concepts developed for dynamic stall analysis,[3] to formulate a realistic mathematical model that can simulate the fluid dynamic processes determining the lateral response of a circular cylinder to Kármán vortex shedding. The detailed analysis is made only for subcritical flow conditions. However, a similar analysis can be made for higher Reynolds numbers. The simulation problems one encounters when using subscale test results are discussed briefly.

Analysis

The detailed investigation by Furguson[1] illustrates the salient features of the cylinder response at subcritical flow conditions. Figure 1 shows that the cylinder response at resonance, $U_\infty \approx 11.5$ fps, is only a fraction of the maximum response at $U_\infty \approx 13.5$ fps. Figure 2 shows that the response below the resonant wind velocity, at $U_\infty = 10.75$ fps, is of the forced oscillation type expected at near-resonant conditions, whereas the response at higher velocity, $U_\infty = 12.4$ fps, shows the buildup to a limit cycle amplitude, which is characteristic of an oscillatory system subject to nonlinear negative damping.[4] The latter type of response is the one occurring when the amplitude exceeds a threshold value and vortex lock-on occurs.[5,6]

Equation of Motion

For a rigid cylinder describing crossflow oscillations, the equation of motion is simply

$$m[\ddot{z} + 2\zeta_0\omega_0\dot{z} + \omega_0^2 z] = \frac{\rho U_\infty^2}{2} D c_f(t) \tag{1}$$

The fluid dynamic lift coefficient $c_f(t)$ can be written as follows using standard linearized formulations:

$$c_f(t) = c_{l\ddot{z}}\frac{\ddot{z}D}{U_\infty^2} + c_{l\dot{z}}\frac{\dot{z}}{U_\infty} + c_{lf}(t) \tag{2}$$

where $c_{lf}(t)$ is the forcing function, generated by the Kármán vortex shedding in the present case.

With ρ_B being the effective mean density of the circular cylinder, one can combine Eqs. (1) and (2) to obtain the following formulation:

$$\ddot{z} + 2\omega_0^* \zeta^* \dot{z} + \omega_0^{*2} z = c_f(t) \tag{3a}$$

where

$$\omega_0^* = \omega_0/\sqrt{1+\rho/\rho_B}$$

$$\zeta^* = [\zeta_0 - (1/\pi\bar{\omega}_0)(\rho/\rho_B)c_{l\dot{z}}]\sqrt{1+(\rho/\rho_B)}$$

Forced Response

For the forced response near resonance, the following conditions exist:

$$c_f(t) = \Delta c_F \sin(\omega_{v0} t)$$

$$\Delta c_F = \frac{2}{\pi}\frac{\rho/\rho_B}{1+\rho/\rho_B}\frac{D\omega_0^2 \Delta c_{lf}}{\bar{\omega}_0^2}$$

$$c_{l\dot{z}} = -c_d \tag{3b}$$

The steady-state response amplitude defined by Eqs. (3a) and (3b) is

$$|z| = \Delta c_F/[\omega_0^{*2} - \omega_{v0}^2)^2 + 4\omega_0^2 \zeta^{*2} \omega_{v0}2]^{\frac{1}{2}} \tag{4}$$

which is maximized at resonance, where $\omega_0^* = \omega_{v0}$

$$\Delta z_{\text{res}} = \frac{\Delta c_F}{2\omega_0^* \omega_{v0}\zeta^*} \tag{5}$$

Using the definitions in Eqs. (3a) and (3b), together with the fact that $\bar{\omega}_0 = 2\pi S_{v0}$, Eq. (5) gives

$$\left(\frac{\Delta z}{D}\right)_{\text{res}} = \frac{(\rho/\rho_B)^*}{4\pi^3 S_{v0}^2}\frac{\Delta c_{lf}}{\zeta_0 + (c_d/2\pi^2 s_{v0})(\rho/\rho_B)^*} \tag{6}$$

where

$$(\rho/\rho_B)^* = (\rho/\rho_B)/\sqrt{1+(\rho/\rho_B)}$$

Δc_{lf} is the amplitude of the forcing function generated by the Kármán vortex shedding on a stationary, nonoscillating cylinder. Figure 3 shows that, for the stationary cylinder, the oscillatory pressure amplitude measured was

$$0.1 < (\Delta C_p)_{v0} < 0.2 \tag{7}$$

It can be seen from Fig. 4 that the fluctuating pressure amplitude dies out fast outside the region 60 deg $\leq \varphi \leq$ 150 deg. As the lift-generating pressure component decreases even faster, one would estimate that the contribution to the lift amplitude is

$$0.05 \leq (\Delta c_{lf})_1 \leq 0.10 \tag{8}$$

provided that the fluctuating pressures on that side are in phase—which they are[1] (Fig. 5). Figure 6 shows that the pressures on the opposite side of the cylinder are of exactly the opposite phase. Thus, the following value of $\Delta c_{lf} = (\Delta c_{lf}) + (\Delta c_{lf})_2$ is indicated by the experimental results.[1]

$$0.1 < \Delta c_{lf} < 0.2 \tag{9}$$

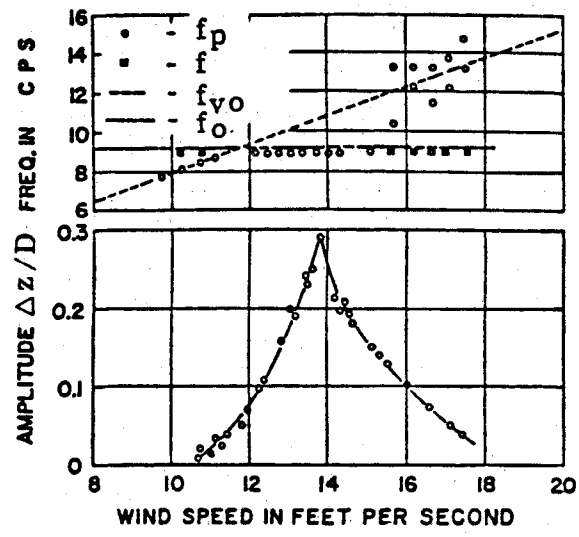

Fig. 1 Response of a circular cylinder to Kármán vortex shedding.[1]

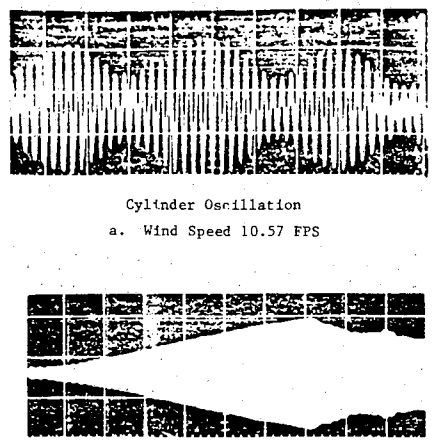

Fig. 2 Response amplitude characteristics below and above resonance.[1]

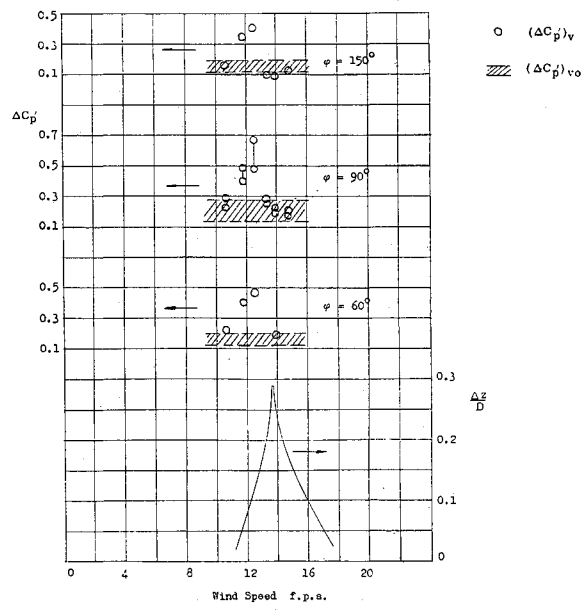

Fig. 3 Fluctuating pressure measurements.[1]

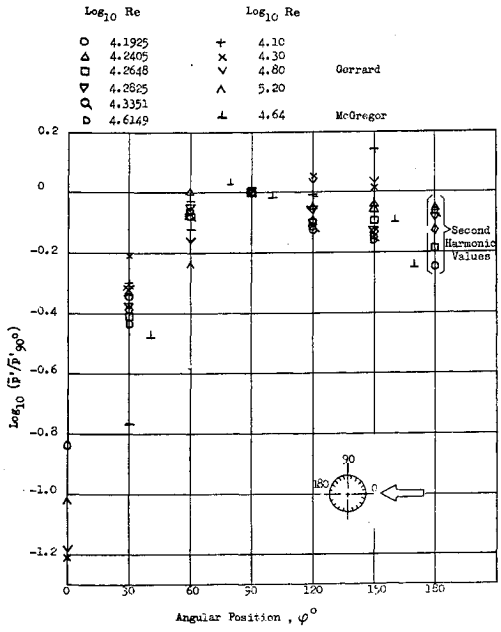

Fig. 4 Circumferential pressure distribution.[1]

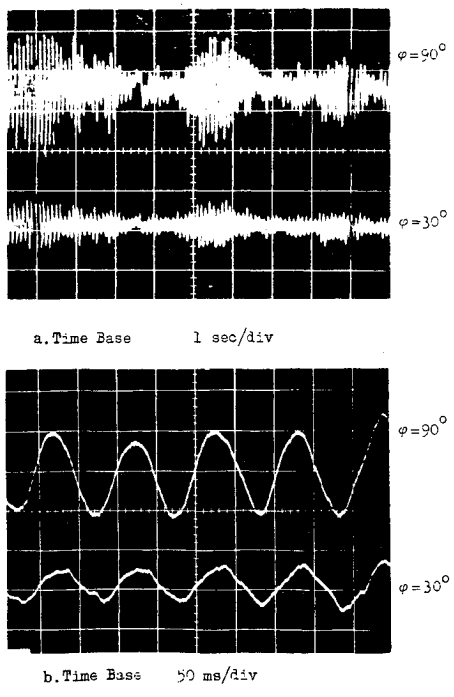

Fig. 5 Adjacent fluctuating pressures.[1]

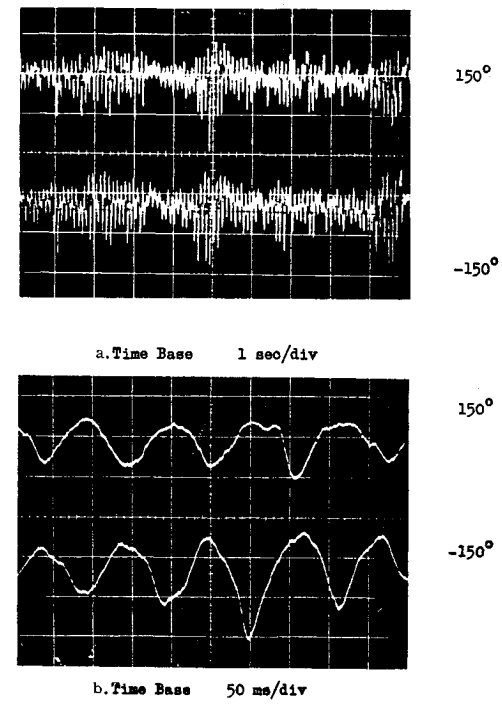

Fig. 6 Fluctuating pressures on opposite sides.[1]

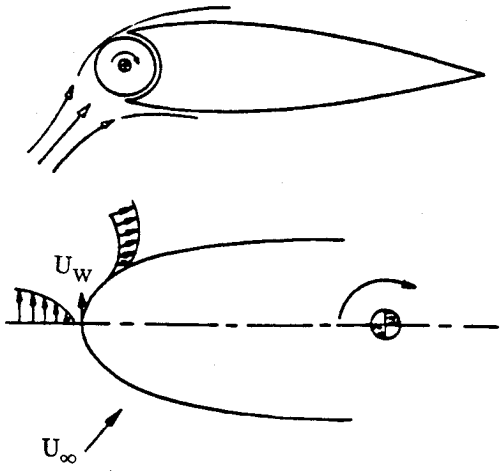

Fig. 7 Moving wall-wall jet analogy.[12]

For Furguson's test at subcritical conditions[1] (Fig. 1), $c_d \approx 1.2$ and $\zeta_0 \approx 0.0012$. For the cylinder itself, $\rho/\rho_B = 0.0156$. However, including the oscillating additional mass gives $\rho/\rho_B = 0.0085$. With those values, Eqs. (6) and (9) give

$$(\Delta z/D)_{\text{res}} = 0.45\,\Delta c_{lf} \tag{10}$$

That is, $0.045 < (\Delta z/D)_{\text{res}} < 0.090$, which is in rather good agreement with the measured resonant response[1] (Fig. 1).

Coupled Response

When the threshold amplitude is exceeded and vortex lock-on occurs, the response is a result of the coupling between body motion and Kármán vortex shedding. Whereas the self-excited response, observed for galloping cables,[7] for example, is as a rule occurring without such coupling effects (see Ref. 8 for exceptions), in the case of the maximum cylinder response in Fig. 1, there is a strong coupling between the unsteady Kármán vortex shedding and the body motion.[9] The flow concept used in Ref. 9 is similar to the "oscillatory Magnus" effect suggested by others,[10,11] although the interpretation is different. The boundary condition at the wall, the so-called "moving wall' effect, and associated change of the flow separation is considered to be the dominant flow phenomenon,[9] not any motion-induced momentum transfer to the inviscid ambient fluid, resulting in a change of the circulation, as has been suggested by others.[10,11]

There is a good deal of similarity between the moving wall effect on dynamic stall[3,12] (Fig. 7) and the effect on a rotating[13] or translating[1] circular cylinder, as pointed out in Refs. 6, 9, and 14 (see Fig. 8). The open vector denotes the lift; the solid vector, the translatory velocity ($\dot{z}$). When the cylinder oscillates slower than the Kármán vortex shedding frequency, the flow separation delay due to the moving wall effect causes negative

aerodynamic damping and will drive the oscillation, just as in the case of the pitching airfoil (Fig. 7).

For the rotating cylinder, the moving wall velocity (U_w) is constant around the circumference. It rotates the mean or time-average orientation of the flow separation, thereby producing a Magnus lift. The unsteady Kármán vortex shedding is present for $U_w/U_\infty < 2$.[15] If the cylinder is describing torsional oscillations at frequencies close to the Kármán vortex shedding frequency, the unsteady separation will, of course, be influenced. The moving wall effect is strongest in the boundary-layer formation region near the stagnation point and becomes weaker further downstream due to increasing boundary-layer thickness and increasing velocity at the edge of the boundary layer. Consequently, the moving wall effect will not differ much for torsional and translational oscillations.

The moving wall effect on the unsteady flow separation will be largest when the cylinder oscillates at a frequency such that the moving wall effect on the "birth" of the boundary layer (at the stagnation point) has been convected to the separation point at the time of flow separation. For other frequencies, the flow separation will be affected by the much weaker moving wall effect existing away from the stagnation point.

Moving Wall Effect

The Kármán vortex shedding on a stationary cylinder generates a fluctuating velocity component $U_\infty \bar{U}_1 \sin\omega t$, which adds to the stationary boundary-layer edge velocity $U_\infty \bar{U}_0$, according to experiments[16] (Fig. 9). The velocity ratio, determining the effect of the moving wall velocity, is $U_w/\bar{U}_e$, where

$$U_e/U_\infty = \bar{U}_0 + \bar{U}_1 \sin\omega t \tag{11}$$

For $\bar{U}_w/U_\infty = 1$, the experimental results in Fig. 9 for U_e/U_∞ define U_w/U_e, as is shown in Fig. 10. In the case of translatory rather than torsional oscillations, U_w becomes

$$U_w = \dot{z}\cos\varphi \tag{12}$$

The time required for convection of the moving wall effect from the stagnation point $\varphi = 0$ to the separation point $\varphi = \varphi_s$ is

$$\Delta t = \varphi_s D/2\bar{U}_c \tag{13}$$

where $\bar{U}_c$ is the mean convection velocity. The mean boundary-layer edge velocity between $\varphi = 0$ and φ_s is given as follows by potential flow theory:

$$\bar{U}_e = \frac{2U_\infty}{\varphi_s}\int_0^{\varphi_s} \sin\varphi \, d\varphi = \frac{2U_\infty}{\varphi_s}(1-\cos\varphi_s) \tag{14}$$

The phase angle $\Delta\phi$ corresponding to Δt, Eq. (13) is,

$$\Delta\phi = 2\pi f \Delta t = \pi S \varphi_s/(\bar{U}_c/U_\infty) \tag{15}$$

For the maximum response, occurring at $\Delta\phi = \pi/2$, Eqs. (14) and (15) give the following value of the corresponding Strouhal number S_m:

$$S_m = \frac{\bar{U}_c}{U_\infty}\Big/ 2\varphi_s = \frac{1-\cos\varphi_s}{\varphi_s^2}\frac{\bar{U}_c}{\bar{U}_e} \tag{16}$$

For subcritical flow conditions, $\varphi_s \approx \pi/2$ and Eq. (16) give

$$S_m = \frac{4}{\pi^2}\frac{\bar{U}_c}{\bar{U}_e} \tag{17}$$

The results in Fig. 1 give $S_m/S_{v0} = 0.83$, which, with $S_{v0} \approx 0.2$, gives the following value for $\bar{U}_c/\bar{U}_e$ from Eq. (17):

$$\bar{U}_c/\bar{U}_e = 0.41 \tag{18}$$

The velocities in a Blasius boundary layer at the displacement and momentum thicknesses, δ^* and θ, respectively, are as follows:[17]

$$U_{\delta^*}/U_e \approx 0.565$$
$$U_\theta/U_e \approx 0.22 \tag{19}$$

Comparing Eqs. (18) and (19) gives

$$\bar{U}_c \approx (U_{\delta^*} + U_\theta)/2 \tag{20}$$

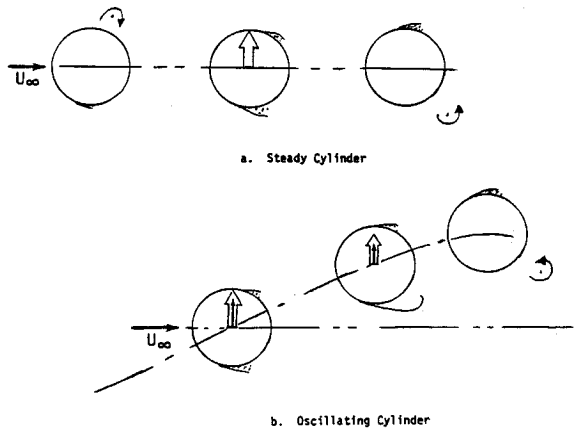

Fig. 8 Unsteady flow separation on steady and oscillating circular cylinder at $f < f_{v0}$.

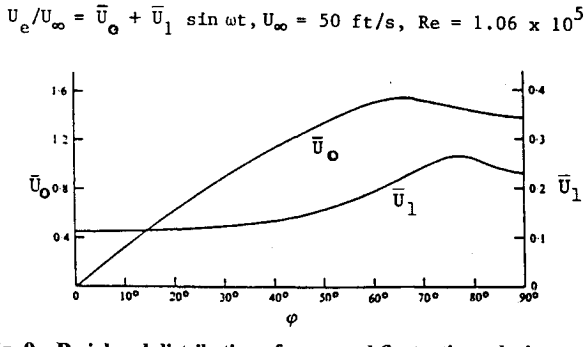

Fig. 9 Peripheral distribution of mean and fluctuating velocity components on a circular cylinder at subcritical flow conditions, $Re = 1.06 \times 10^6$.[16]

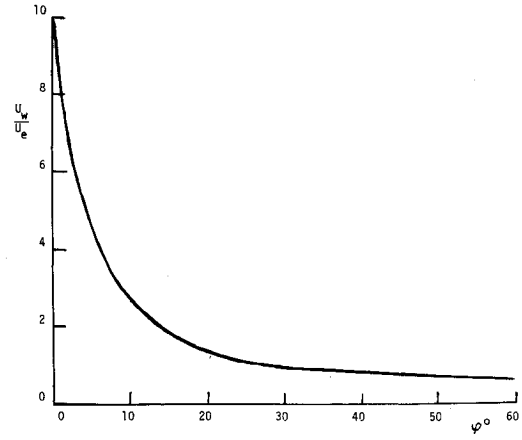

Fig. 10 Velocity ratio U_w/U_e as a function of peripheral angle φ for $U_w = U_\infty$.

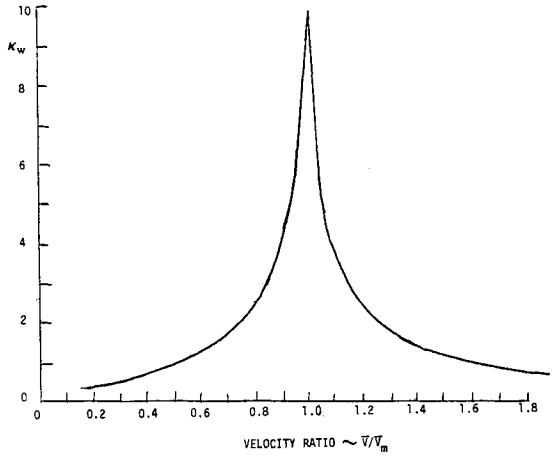

Fig. 11 Computed variation of the moving wall effect κ_w for $U_w/U_\infty = 1$.

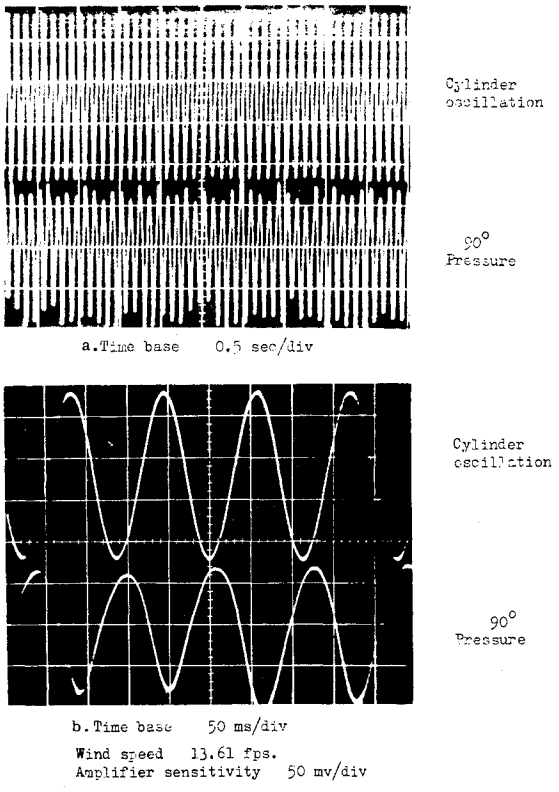

Fig. 12 Measured maximum pressure amplitude during vortex lock-on.[19]

For other frequencies, $S \neq S_m$, the moving wall effect reaching φ_s at the time of separation was generated at $\varphi = \varphi_0 \neq 0$. Substituting $\varphi = 0$ with $\varphi = \varphi_0$ in Eq. (14) gives

$$\bar{U}_e = \frac{2U_\infty}{\varphi_s - \varphi_0}\int_{\varphi_0}^{\varphi_s} \sin\varphi \, d\varphi = \frac{2U_\infty}{\varphi_s - \varphi_0}(\cos\varphi_0 - \cos\varphi_s) \tag{21}$$

Combining Eq. (21) with Eq. (15), where for maximum moving wall effect $\Delta\phi = \pi/2$, one obtains

$$\varphi_s - \varphi_0 = \frac{1}{2S}\frac{\bar{U}_c}{\bar{U}_e}\frac{\bar{U}_e}{U_\infty} = \frac{\bar{U}_c}{\bar{U}_e}\frac{\cos\varphi_0 - \cos\varphi_s}{S(\varphi_s - \varphi_0)} \tag{22}$$

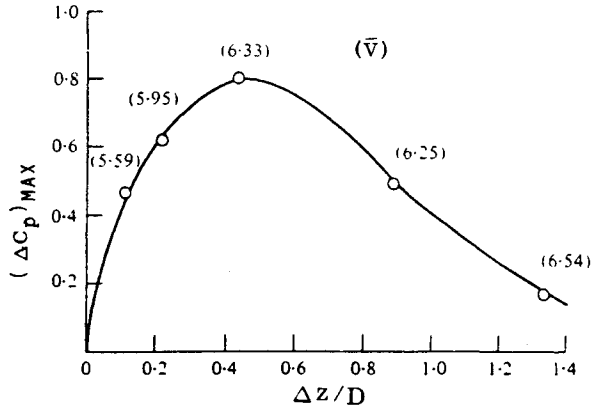

Fig. 13 Predicted and measured subcritical response to Kármán vortex shedding.

For φ_0 small, Eq. (22) can be approximated to give

$$\varphi_0 \approx \varphi_s - \sqrt{(\bar{U}_c/\bar{U}_e)(1 - \cos\varphi_s)\bar{V}} \tag{23}$$

where $\bar{V} = S^{-1}$.

At $\varphi = \varphi_0$, the boundary-layer edge velocity is

$$U_e/U_\infty = \bar{U}_0 + \bar{U}_1 \sin 2\pi f_v t \tag{24}$$

where $\bar{U}_0$ is defined by potential flow theory as $\bar{U}_0 = 2\sin\varphi$, and $\bar{U}_1 \approx 0.1$, according to experiments[16] (Fig. 9). For vortex lock-on, the shedding phenomenon of interest, $f_v = f_0$, and U_w is in phase with $\bar{U}_1 \sin 2\pi f_v t$. When φ_0 is small and $\bar{U}_1 \sin 2\pi f_v t$ dominates in Eq. (24), $|U_w|/U_e \approx |U_w|/U_1$. When φ_0 is not small, $\bar{U}_0$ dominates, and $|U_w|/U_e \approx |U_w|/\bar{U}_0$. Consequently, the relative magnitude $|U_w|/|U_e|$ can be estimated as follows:

$$\frac{|U_w|}{|U_e|} = \frac{|\dot{z}|}{U_\infty}\frac{\cos\varphi_0}{2\sin\varphi_0 + 0.1} \tag{25}$$

with $\varphi_s \approx \pi/2$, Eq. (23) gives

$$\varphi_0 = \pi/2 - \sqrt{(\bar{U}_c/\bar{U}_e)\bar{V}} \tag{26}$$

Combining Eqs. (25) and (26), the results shown in Fig. 11 are obtained for the relative magnitude of the moving wall effect, $\kappa_w = (|U_w|/|U_e|)/(|\dot{z}|/U_\infty)$. Comparing Figs. 1 and 11, it is obvious that the relative moving wall effect κ_w gives a good representation of the variation of the response amplitude with velocity during vortex lock-on. The next step is, of course, to try to predict the experimental response.

During lock-on, the vortex shedding is controlled by the body motion ($S_{v0} = S_0$), and the forcing function $c_f(t)$ in Eq. (3) vanishes. That is, the forced oscillation response converts to a limit cycling phenomenon, with the limit cycle amplitude determined by $\zeta^* = 0$, where

$$\zeta^* = \left[\zeta_0 - \frac{1}{\pi\bar{\omega}_0}(\rho/\rho_B)c_{l\bar{z}}\right]\Big/\sqrt{1 + (\rho/\rho_B)} \tag{27}$$

That is, the linear damping term $c_{l\dot{z}}$ in Eq. (3) is substituted by an effective damping term $c_{l\bar{z}}$, representing the integrated nonlinear damping in derivative form. Expanding on Scruton's analysis,[18] one can represent $c_{l\bar{z}}$ as follows:

$$c_{l\bar{z}} = c_{l\dot{z}} + \frac{\Delta c_{lD}}{|\dot{z}|/U_\infty} \tag{28}$$

$c_{l\dot{z}}$ is the damping derivative for the linear case, Eq. (3). It is generated by the rotation of the drag vector, which gives the

following lift:

$$c_l(\dot{z}) = -c_d(\dot{z}/U_\infty)\sqrt{1+(\dot{z}/U_\infty)^2} \tag{29}$$

Differentiating Eq. (29) gives

$$c_{l\dot{z}} = \frac{\partial c_l(\dot{z})}{\partial(\dot{z}/V)} = -c_d \frac{1+2(\dot{z}/U_\infty)^2}{\sqrt{1+(\dot{z}/U_\infty)^2}} \tag{30}$$

where $|\dot{z}|/U_\infty = 2\pi S_0\, \Delta z/D$.

Combining Eqs. (27) and (30) gives

$$\zeta^* \sqrt{1+\frac{\rho}{\rho_B}} = \zeta_0 + \frac{1}{2\pi^2 S_0}\frac{\rho}{\rho_B}\left[c_d^* - \frac{\Delta c_{lD}}{|\dot{z}|/U_\infty}\right] \tag{31}$$

where $c_d^* = c_d[1+2(2\pi S_0\, \Delta z/D)^2]/[1+(2\pi S_0\, \Delta z/D)^2]^{\frac{1}{2}}$.

The maximum limit cycle amplitude, determined by $\zeta^* = 0$, is

$$\left(\frac{\Delta z}{D}\right)_{\max} = \frac{\rho/\rho_B}{4\pi^3 S_0^2}\frac{(\Delta c_{lD})_{\max}}{\zeta_0 + (c_d^*/2\pi^2 S_0)(\rho/\rho_B)} \tag{32}$$

For an initial estimate of $(\Delta z/D)_{\max}$, $c_d^* = c_d$ is used in Eq. (32). Using this amplitude value, c_d^* is computed for each iterative step until the final converged value of $(\Delta z/D)_{\max}$ is obtained.

The experimental results obtained by Bearman and Currie[19] gave the results shown in Fig. 12. The maximum pressure amplitude at $\varphi = 90$ deg is $\Delta C_p \approx 0.8$. Based on the discussion earlier for the pressure fluctuations on the stationary cylinder, one expects

$$(\Delta c_{lD})_{\max} \approx 0.8 \tag{33}$$

For Furguson's test, with $\rho/\rho_B = 0.0085$, $\zeta_0 = 0.0012$, and $S_0 = S_{v0} = 0.198$, Eqs. (31–33) give the following final value of $(\Delta z/D)_{\max}$:

$$(\Delta z/D)_{\max} = 0.32 \tag{34}$$

This upper limit for the lock-on response is in rather good agreement with the measured response,[1] $(\Delta z/D)_{\max} \approx 0.30$ (Fig. 1). Combining this with the results of Eq. (25) (Fig. 11) provides a method for prediction of the cylinder response over the complete reduced velocity domain, $\bar{V} = S^{-1}$.

$$(\Delta z/D)_{\text{lim}} = (\Delta z/D)_{\max}\kappa_w/(\kappa_w)_{\max} = 0.32\kappa_w/(\kappa_w)_{\max} \tag{35}$$

provided that $\bar{V} > (1+\epsilon)\bar{V}_{\text{res}}$.

For the near-resonant response at $\bar{V} \le (1+\epsilon)\bar{V}_{\text{res}}$, Eqs. (3a), (3b), and (4) give

$$\frac{\Delta z}{D}\Big/\left(\frac{\Delta z}{D}\right)_{\text{res}} = \left\{\left(\frac{\bar{V}_0}{\bar{V}_{v0}}\right)^2 + \frac{1}{2\zeta^*}\left[1-\left(\frac{\bar{V}_0}{\bar{V}_{v0}}\right)^2\right]^2\right\}^{-\frac{1}{2}} \tag{36}$$

Combining Eqs. (35) and (36) with the results shown earlier in Eqs. (10), (25), and (26) gives the prediction shown in Fig. 13 for Furguson's test.[1] As can be seen, the agreement between prediction and experimental results is rather good. Apparently, the lower bound for the near-resonant response, Eq. (7), applies. The falloff of the experimental results at $\bar{V} > 7$ is due to the cessation of vortex lock-on (see Fig. 1).

Having the analytical tools, one can now evaluate to what degree the presence of mechanical damping, $\zeta_0 = 0.0012$, in the test did affect the measured response (Fig. 14). As can be seen, the response amplitudes would have been roughly 50% larger in the absence of mechanical damping. To keep the mechanical damping down to 0.12% of critical in a wind tunnel test is a real achievement. However, even in that case, the effect on the measured response can be large, as is illustrated by Fig. 14. This demonstrates the difficulties encountered when trying to simulate the dynamic response in a wind-tunnel test. In addition, there are other problems associated with trying to apply subscale test data to full-scale structures.

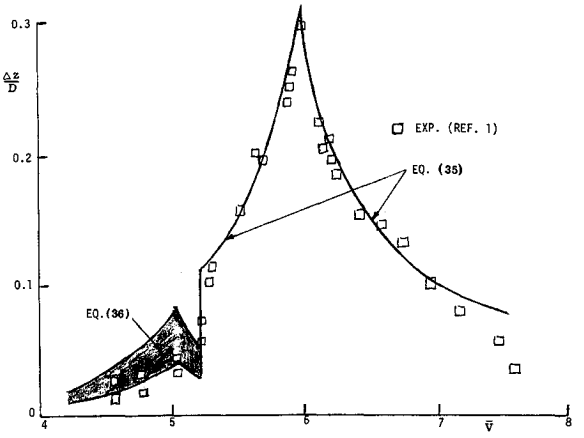

Fig. 14 Effect of mechanical damping on response amplitude.

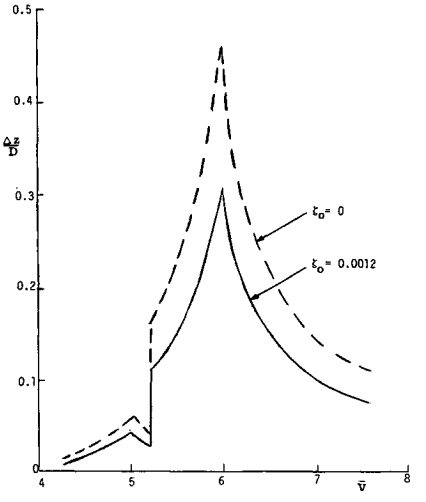

Fig. 15 Effect of mechanical damping on response amplitude.

Simulation Difficulties

The usual simulation difficulties encountered in subscale dynamic tests[20,21] will, of course, be present. Based on the experience with bodies of revolution at high angles of attack,[22,23] one would expect the response characteristics to change dramatically when going through the critical flow regime. Even at high, transcritical Reynolds numbers, when the slender-body vortex shedding becomes similar in character to that for subcritical flow conditions,[24] large differences still remain in regard to the unsteady response to Kármán vortices of a two-dimensional circular cylinder. This is because of the changed convection velocity, Eq. (20), which is too high at transcritical flow conditions to permit the optimum phasing, which occurs in subcritical flow.

Conclusions

An analysis of the circular cylinder response to Kármán vortex shedding has given results that can be summarized as follows:

1) The cylinder response has two distinctly different characteristics, depending on the closeness to the resonant flow condition. Below and slightly above the resonant velocity, the cylinder response is of the forced response type. At higher velocities, coupling occurs between the cylinder motion and the flow separation (and associated vortex shedding), resulting in greatly increased response amplitudes.

2) The coupling in this vortex lock-on region is caused by so-called moving wall effects. By applying unsteady flow concepts developed earlier for dynamic stall, the response measured during vortex lock-on at subcritical flow conditions can be predicted with good accuracy.

3) It is noted that the dynamic simulation problems existing in subscale tests are aggravated in the present case due to the effect of the boundary-layer characteristics on the phasing between body motion and Kármán vortex shedding.

References

[1]Furguson, N., "The Measurement of Wake and Surface Effects in the Subcritical Flow Past a Circular Cylinder at Rest and in Vortex-Excited Oscillation," M.A.Sc. thesis, Univ. of British Columbia, Canada, Sept. 1965.

[2]Furguson, N. and Parkinson, G. V., "Surface and Wake Phenomena of the Vortex Excited Oscillation of a Circular Cylinder," *Journal of Engineering for Industry*, Vol. 89, Nov. 1967, pp. 831–838.

[3]Ericsson, L. E. and Reding, J. P., "Unsteady Flow Concepts for Dynamic Stall Analysis," *Journal of Aircraft*, Vol. 21, Aug. 1984, pp. 601–606.

[4]Ericsson, L. E., "Unsteady Aerodynamics of Separating and Reattaching Flows on Bodies of Revolution," *Recent Research on Unsteady Boundary Layers*, Vol. 1, IUTAM Symposium, Laval Univ., Quebec, May 1971, pp. 481–512.

[5]Ogawa, A. and Nakagawa, K., "Stability of the Vortex Sheet in the Wake of Stationary and Vibrating Cylinders," *Transactions of the Japan Society of Aerospace Science*, Vol. 20, Feb. 1978, pp. 167–176.

[6]Ericsson, L. E., "Maximum Crossflow Response of a Circular Cylinder, a Non-Resonant Flow Phenomenon," AIAA Paper 84-0422, Jan. 1984,

[7]Ericsson, L. E., "Limit Amplitude of Galloping Bluff Cylinders," *AIAA Journal*, Vol. 22, April 1984, pp. 493–497.

[8]Ericsson, L. E., "Karman Vortex Shedding, Friend or Foe of the Structural Dynamicist," *Journal of Aircraft*, Vol. 23, Aug. 1986, pp. 621–628.

[9]Ericsson, L. E., "Karman Vortex Shedding and the Effect of Body Motion," *AIAA Journal*, Vol. 18, Aug. 1980, pp. 935–944.

[10]Morris, A. W., "A Review on Vortex Sheets, Periodic Wakes, and Induced Vibration Phenomena," *Journal of Basic Engineering*, Vol. 86, June 1964, pp. 185–196.

[11]Bublitz, P., "The Periodic Normal Force on a Circular Cylinder in Cross Flow—An Unsteady Magnus Effect," *Z. Flugwiss. Weltraumforsch.* 7 (1983), Heft 4, pp. 253–262.

[12]Ericsson, L. E. and Reding, J. P., "Analytic Prediction of Dynamic Stall Characteristics," AIAA Paper 72-682, June 1972.

[13]Swanson, W. M., "The Magnus Effect: A Summary of Investigations to Date," *Journal of Basic Engineering*, Vol. 83, Sept. 1961, pp. 461–470.

[14]Ericsson, L. E., "Fluid Dynamics of Cylinder Response to Karman Vortex Shedding," AIAA Paper 86-0119, Jan. 1986.

[15]Diaz, F., Gavalda', J., Kawall, J. G., Keller, J. F., and Giralt, F., "Vortex Shedding from a Spinning Cylinder," *Physics of Fluids*, Vol. 26, Dec. 1983, pp. 3454–3460.

[16]Dwyer, H. A. and McCroskey, W. J., "Oscillating Flow Over a Cylinder at Large Reynolds Number," *Journal of Fluid Mechanics*, Vol. 61, Pt. 4, 1973, pp. 753–767.

[17]Schlichting, H., *Boundary Layer Theory*, translated by J. Kestin, McGraw-Hill, London, 1955.

[18]Scruton, C., "On the Wind Excited Oscillations of Stacks, Towers and Masts," Paper 16, International Conference on Wind Effects and Buildings and Structures, NPL, England, June 1963.

[19]Bearman, P. W. and Currie, I. G., "Pressure Fluctuation Measurements on an Oscillating Circular Cylinder," *Journal of Fluid Mechanics*, Vol. 91, Pt. 4, 1979, pp. 661–677.

[20]Ericsson, L. E. and Reding, J. P., "Scaling Problems in Dynamic Tests of Aircraft-like Configurations," Paper 25, AGARD-CP-227, Feb. 1978.

[21]Ericsson, L. E. and Reding, J. P., "Reynolds Number Criticality in Dynamic Tests," AIAA Paper 78-166, Jan. 1978.

[22]Ericsson, L. E. and Reding, J. P., "Steady and Unsteady Vortex-Induced Asymmetric Loads on Slender Vehicles," *Journal of Spacecraft and Rockets*, Vol. 18, March-April 1981, pp. 97–109.

[23]Ericsson, L. E. and Reding, J. P., "Dynamics of Forebody Flow Separation and Associated Vortices," *Journal of Aircraft*, Vol. 22, April 1985, pp. 329–335.

[24]Reding, J. P. and Ericsson, L. E., "A Re-examination of the Maximum Normalized Vortex-Induced Side Force," *Journal of Spacecraft and Rockets*, Vol. 21, Sept.-Oct. 1984, pp. 433–440.